NATIONAL AERONAUTICS AND SPACE ADMINISTRATION

Technical Memorandum 33-498

Magnetic Materials Selection for Static Inverter and Converter Transformers

Colonel W. T. McLyman

JET PROPULSION LABORATORY
CALIFORNIA INSTITUTE OF TECHNOLOGY
PASADENA, CALIFORNIA

November 1, 1971

NATIONAL AERONAUTICS AND SPACE ADMINISTRATION

Technical Memorandum 33-498

Magnetic Materials Selection for Static Inverter and Converter Transformers

Colonel W. T. McLyman

JET PROPULSION LABORATORY
CALIFORNIA INSTITUTE OF TECHNOLOGY
PASADENA, CALIFORNIA

November 1, 1971

PREFACE

The work described in this report was performed by the Guidance and Control Division of the Jet Propulsion Laboratory.

ACKNOWLEDGMENT

The author wishes to express his thanks to Dr. S. J. Lindena of Electro-Optical Systems, R. G. Noah of Magnetic Inc., and K. L. Latimer of Arnold Engineering for support in gathering data and technical aid.

CONTENTS

CONTENTS (contd)

FIGURES (contd)

CONTENTS (contd)

FIGURES (contd)

ABSTRACT

A program was conducted to study magnetic materials for use in spacecraft transformers used in static inverters, converters, and transformer-rectifier supplies. Different magnetic alloys best suited for high-frequency and high-efficiency applications were comparatively investigated together with an investigation of each alloy's inherent characteristics.

The materials evaluated were:

Trade name	Magnetic alloys
Orthonol	50% Ni, 50% Fe
Sq. Permalloy	79% Ni, 17% Fe, 4% Mo
48 alloy	48% Ni, 52% Fe
Supermalloy	78% Ni, 17% Fe, 5% Mo
Magnesil	3% Si, 97% Fe

One of the characteristics in magnetic materials detrimental in transformer design is the residual flux density, which can be additive on turn-on and cause the transformer to saturate. Investigation of this problem led to the design of a transformer with a very low residual flux. Tests were performed to determine the dc and ac magnetic properties at 2400 Hz using square-wave excitation. These tests were performed on uncut cores, which were then cut for comparison of the gapped and ungapped magnetic properties. When the data of many transformers in many configurations were compiled the optimum transformer was found to be that with the lowest residual flux and a small amount of air gap in the magnetic material. The data obtained from these tests are described, and the potential uses for the materials are discussed.

I. INTRODUCTION

Transformers used in static inverters, converters and transformer-rectifier (T-R) supplies intended for spacecraft power applications are usually of square loop toroidal design. The design of reliable, efficient, and lightweight devices of this class for such use has been seriously hampered by the lack of engineering data describing the behavior of both the commonly used and the more exotic core materials with higher frequency square wave excitation.

A program has been carried out at JPL to study this data. An investigation has been made to ascertain the dynamic B-H loop characteristics of the different core materials presently available from various industry sources. Cores were procured in both toroidal and "C" forms and were tested in both ungapped (uncut) and gapped (cut) configurations. The following describes the results of this investigation.

II. TYPICAL OPERATION

Transformers used for inverters, converters, and I-R supplies operate from the spacecraft power bus, which could be dc or ac. In some power applications, a commonly used circuit is a driven transistor switch arrangement such as that shown in Fig. 1.

One important consideration affecting the design of suitable transformers is that care must be taken to ensure that operation involves balanced drive to the transformer primary. In the absence of balanced drive, a net dc current will flow in the transformer primary, which causes the core to saturate easily during alternate half-cycles. A saturated core cannot support the applied voltage, and, because of lowered transformer impedance, the current flowing in a switching transistor is limited only by its beta. The resulting high current, in conjunction with the transformer leakage inductance, results in a high voltage spike during the switching sequence that could be destructive to the transistors. To provide balanced drive, it is necessary to exactly match the transistors for V_{CE} (SAT) and beta, and this is not always sufficiently effective. Also, exact matching of the transistors is a major problem in the practical sense.

III. MATERIAL CHARACTERISTICS

Many available core materials approximate the ideal square loop characteristic illustrated by the B-H curve shown in Fig. 2.

Representative dc B-H loops for commonly available core materials are shown in Fig. 3. Other characteristics are tabulated in Table 1.

Many articles have been written about inverter and converter transformer design. Usually, the author's recommendation represents a compromise among material characteristics such as those tabulated in Table 1 and displayed in Fig. 3. These data are typical of commercially available core materials that are suitable for the particular application.

As can be seen, the material that provides the highest flux density (silicon) would result in smallest component size, and this would influence the choice, if size were the most important consideration. The type 78 material (see the 78% curve in Fig. 3) has the lowest flux density. This results in the largest size transformer, but, on the other hand, this material has the lowest coercive force and the lowest core loss of any other core material available.

Usually, inverter transformer design is aimed at the smallest size, with the highest efficiency, and adequate performance under the widest range of environmental conditions. Unfortunately, the core material that can produce the smallest size has the lowest efficiency. The highest efficiency materials result in the largest size. Thus the transformer designer must make tradeoffs between allowable transformer size and the minimum efficiency that can be tolerated. The choice of core material will then be based upon achieving the best characteristic on the most critical or important design parameter, and acceptable compromises on the other parameters.

Based upon analysis of past design performance, most engineers select size rather than efficiency as the most important criteria and select an intermediate core material for their designs. Consequently, square loop 50-50 nickel-iron has become the most popular material.

IV. CORE SATURATION DEFINITION

To standardize the definition of saturation, several unique points on the B-H loop are defined as shown in Fig. 4.

The straight line through (H_0, 0) and (H_s, B_s) may be written as:

$$B = \left(\frac{dB}{dH}\right)(H - H_0) \tag{1}$$

The line through (0, B_s) and (H_s, B_s) has essentially zero slope and may be written as:

$$B = B_2 \approx B_s \tag{2}$$

Equations (1) and (2) together defined "saturation" conditions as follows:

$$B_s = \left(\frac{dB}{dH}\right)(H_s - H_0) \tag{3}$$

Solving Eq. (3) for H_s,

$$H_s = H_0 + \frac{B_s}{\mu_0} \tag{4}$$

where

$$\mu 0 = \frac{dB}{dH}$$

by definition.

Saturation occurs when the peak exciting current is twice the average exciting current as shown in Fig. 5. Analytically this means that:

$$H_{pK} = 2H_s \tag{5}$$

Solving Eq. (1) for H_1, we obtain

$$H_1 = H_0 + \frac{B_1}{\mu_0} \tag{6}$$

To obtain the presaturation dc margin (ΔH), Eq. (4) is subtracted from Eq. (3):

$$\Delta H = H_s - H_1 = \frac{B_s - B_1}{\mu_0} \tag{7}$$

The actual unbalanced dc current must be limited to

$$I_{DC} \leq \frac{\Delta H}{N\ell} \text{ (amperes)} \tag{8}$$

where

N = TURNS

ℓ = mean magnetic length

Combining Eqs. (7) and (8) gives

$$I_{DC} \leq \frac{B_s - B_1}{\mu_0 N\ell} \text{ (amperes)} \tag{9}$$

As mentioned earlier, in an effort to prevent core saturation, the switching transistors are matched for beta and $V_{CE}(SAT)$ characteristics. The effect of core saturation using an uncut or ungapped core is shown in Fig. 6, which illustrates the effect on the B-H loop when traversed with a dc bias. Figure 7 shows typical B-H loops of 50-50 nickel-iron excited from an ac source with progressively reduced excitation; the vertical scale is 0.4 T/cm. It can be noted that the minor loop remains at one extreme position within the B-H major loop after reduction of excitation. The unfortunate effect of this random minor loop positioning is that when conduction again begins in the transformer winding after shutdown, the flux swing could begin from the extreme, and not from the normal zero axis. The effect of this is to drive the core into saturation with the production of spikes that can destroy transistors.

V. THE TEST SETUP

A test fixture, schematically indicated in Fig. 8, was built to effect comparison of dynamic B-H loop characteristics of various core materials. Cores were fabricated from various core materials in the basic core configuration designated No. 52029 for toroidal cores manufactured by Magnetics, Inc. The materials used were those most likely to be of interest to designers of inverter or converter transformers. Test conditions are listed in Table 2. Winding data was derived from the following:

$$N_T = \frac{V \cdot 10^4}{4.0 \cdot B_m \cdot F \cdot A_c}$$

where

N_T = Number of turns

B_m = Flux density, T

F = Frequency, Hz

A_c = Core area, cm^2

V = Voltage

The test transformer represented in Fig. 9 consists of 54-turn primary and secondary windings, with square wave excitation on the primary. Normally switch S1 is open. With switch S1 closed, the secondary current is rectified by the diode to produce a dc bias in the secondary winding.

Cores were fabricated from each of the materials by winding a ribbon of the same thickness on a mandrel of a given diameter. Ribbon termination was effected by welding in the conventional manner. The cores were vacuum impregnated, baked, and finished as usual.

Figures 10, 11, 12, 13 and 14 show the dynamic B-H loops obtained for the different core materials designated therein. Figure 15 shows a

composite of all the B-H loops. In each of these, switch S1 was in the open position so that there was no dc bias applied to the core and windings.

The photographs designated Figures 16, 17, 18, 19 and 20 show the dynamic B-H loop patterns obtained for the designated core materials when the test conditions included a sequence in which switch S1 was open, then closed, and then opened. It is apparent from these views that with a small amount of dc bias, the minor dynamic B-H loop can traverse the major B-H loop from saturation to saturation. In Figs. 16 to 18, it will be noted that after the dc bias had been removed, the minor B-H loops remained shifted to one side or the other. Because of ac coupling of the current to the oscilloscope, the photographs do not present a complete picture of what really happens during the flux swing.

VI. CORE SATURATION THEORY

The domain theory of the nature of magnetism is based on the assumption that all magnetic materials consist of individual molecular magnets. These minute magnets are capable of movement within the material. When a magnetic material is in its unmagnetized state, the individual magnetic particles are arranged at random, and effectively neutralize each other. An example of this is shown in Fig. 21, where the tiny magnetic particles are arranged in a disorganized manner. The north poles are represented by the darkened ends of the magnetic particles. When a material is magnetized, the individual particles are aligned or oriented in a definite direction (Fig. 22).

The degree of magnetization of a material depends on the degree of alignment of the particles. The external magnetizing force can continue up to the point of saturation, that is, the point at which essentially all of the domains are lined up in the same direction.

In a typical toroid core, the effective air gap is less than 10^{-6} cm. Such a gap is negligible in comparison to the ratio of mean length to permeability. If the toroid were subjected to a strong magnetic field (enough to saturate), essentially all of the domains would line up in the same direction.

If suddenly the field were removed at B_m, the domains would remain lined up and be magnetized along that axis. The amount of flux density that remains is called residual flux or B_r. The result of this effect was shown earlier in Figs. 16 to 18.

VII. AIR GAP

An air gap introduced into the core has a powerful demagnetizing effect, resulting in "shearing over" of the hysteresis loop and a considerable decrease in permeability of high-permeability materials. The dc excitation follows the same pattern. However, the core bias is considerably less affected by the introduction of a small air gap than the magnetization characteristics. The magnitude of the air gap effect also depends on the length of the mean magnetic path and on the characteristics of the uncut core. For the same air gap, the decrease in permeability will be less with a greater magnetic flux path but more pronounced in a low coercive force, high-permeability core.

VIII. EFFECT OF GAPPING

Figure 23 shows a comparison of a typical toroid core B-H loop without and with a gap. The gap increases the effective length of the magnetic path. When voltage E is impressed across primary winding N_1 of a transformer, the resulting current i_m will be small because of the highly inductive circuit shown in Fig. 24. For a particular size core, maximum inductance occurs when the air gap is minimum.

When S1 is closed, an unbalanced dc current flows in the N_2 turns and the core is subjected to a dc magnetizing force, resulting in a flux density that may be expressed as

$$B_{dc} = \frac{1.25\ N\ I_{dc} \times 10^{-4}}{\ell_g + \frac{\ell_m}{\mu_{dc}}} \text{ (teslas)}$$

where

ℓ_m = Mean length, cm

ℓ_g = Gap, cm

B_{dc} = dc flux density, T

I_{dc} = Unbalanced direct current, A

μ_{dc} = dc permeability

N = Number of turns

In converter and inverter design, this is augmented by the ac flux swing, which is:

$$B_{ac} = \frac{E \cdot 10^4}{K \cdot F \cdot AC \cdot N} \text{ (teslas)}$$

where

B_{ac} = ac flux density, T

E = ac voltage

F = Frequency, Hz

A_C = Core area, cm^2

K = 4.0 for a square wave

K = 4.4 for a sine wave

N = Number of turns

If the sum of B_{dc} and B_{ac} shifts operation above the maximum operating flux density of the core material, the incremental permeability (μac) is reduced. This lowers the impedance and increases the flow of magnetizing current i_m. This can be remedied by introducing an air gap into the core assembly, which effects a decrease in dc magnetization in the core. However, the amount of air gap that can be incorporated has a practical limitation since the air gap lowers impedance, which results in increased magnetizing current (i_m). The magnetizing current is inductive in nature. The resultant voltage spikes produced by such currents apply a great stress to the switching transistors, and may cause failure. This can be minimized by tight control of lapping and etching of the gap to keep the gap to a minimum.

From Fig. 23, it can be seen that the B-H curves depict maximum flux density B_m and residual flux B_r for ungapped and gapped cores, and that the useful flux swing is designated ΔB, which is the difference between them. It will be noted in Fig. 23a that B_r approaches B_m, but that in Fig. 23b there is a much greater ΔB between them. In either case, when excitation voltage is removed at the peak of the excursion of the B-H loop, flux falls to the B_r point. It is apparent that introducing an air gap then reduces B_r to a lower level, and increases the useful flux density. Thus insertion of an air gap in the core eliminates, or reduces markedly, the voltage spikes produced by the leakage inductance due to the transformer saturation.

Two types of core configurations were investigated in the ungapped and gapped states. Figure 25 shows the type of toroidal core that was cut and Fig. 26 shows the type of C core that was cut. Toroidal cores as conventionally fabricated are virtually gapless. To increase the gap, the cores were physically cut in half and the cut edges were lapped, acid etched to remove cut debris, and banded to form the cores. A minimum air gap on the order of less than 25 μm was established.

As will be noted from Figs. 27 to 31, which show the B-H loops of the uncut and cut cores, the results obtained indicated that the effect of gapping was the same for both the C-cores and the toroidal cores subjected to testing. It will be noted however, that gapping of the toroidal cores produced a lowered squareness characteristic for the B-H loop as shown in Table 3; this data was obtained from Figs. 27 to 31. Also, from Figs. 27 to 31, ΔH was extracted as shown in Fig. 32 and tabulated in Table 4.

A direct comparison of cut and uncut cores was made electrically by means of two different circuit configurations. The magnetic material used in this branch of the test was Orthonol. The operating frequency was 2.4 kHz, and the flux density was 0.6 T. The first circuit, shown in Fig. 33, was a driven inverter operating into a 30 W load, with the transistors operating into and out of saturation. Drive was applied continuously. S1 controls the supply voltage to Q1 and Q2.

With switch S1 closed, transistor Q1 was turned on and allowed to saturate. This applied $E-V_C(SAT)$ across the transformer winding. Switch S1 was then opened. The flux in transformer T2 then dropped to the residual flux density B_r. Switch S1 was closed again. This was done several times in succession to catch the flux in an additive direction. Figures 34 and 35 show the inrush current measured at the center tap of T2.

It will be noted in Fig. 34 that the uncut core saturated and that inrush current was limited only by circuit resistance and transistor beta. It can be noted in Fig. 35 that saturation did not occur in the case of the cut core. The high inrush current and transistor stress was thus virtually eliminated.

The second test circuit arrangement is shown in Fig. 36. The purpose of this test was to excite a transformer and catch the inrush current using a current probe. A square wave power oscillator was used to excite transformer T2. Switch S1 was opened and closed several times to catch the flux in an additive direction. Figures 37 and 38 show inrush current for a cut and uncut core respectively.

A small amount of air gap, less than 25 μm, has a powerful demagnetizing effect and this gap has little effect on core loss. This small amount of air gap decreases the residal magnetism by "shearing over" the hysteresis loop. This eliminated the ability of the core to remain saturated.

A typical example showing the merit of the cut core was in the checkout of a Mariner spacecraft. During the checkout of a prototype science package, a large (8 A, 200 μs) turn-on transient was observed. The normal running current was 0.06 A, and was fused with a parallel-redundant 1/8-A fuse as required by the Mariner Mars 1971 design philosophy. With this 8-A inrush current, the 1/8-A fuses were easily blown. This did not happen on every turn-on, but only when the core would "latch up" in the wrong direction for turn-on. Upon inspection, the transformer turned out to be a 50-50 Ni-Fe toroid. The design was changed from a toroidal core to a cut-core with a 25-μm air gap. The new design was completely successful in eliminating the 8-A turn-on transient.

IX. SUMMARY

Low-loss tape-wound toroidal core materials that have a very square hysteresis characteristic (B-H loop) have been used extensively in the design of spacecraft transformers. Due to the squareness of the B-H loops of these materials, transformers designed with them tend to saturate quite easily. As a result, large voltage and current spikes, which cause undue stress on the electronic circuitry, can occur. Saturation occurs when there is any unbalance in the ac drive to the transformer, or when any dc excitation exists. Also, due to the square characteristic, a high residual flux state (B_r) may remain when excitation is removed. Reapplication of excitation in the same direction may cause deep saturation and an extremely large current spike, limited only by source impedance and transformer winding resistance, can result. This can produce catastrophic results.

By introducing a small (less than 25-μm) air gap into the core, the problems described above can be avoided and, at the same time, the low-loss properties of the materials retained. The air gap has the effect of "shearing over" the B-H loop of the material such that the residual flux state is low and the margin between operating flux density and saturation flux density is high. The air gap thus has a powerful demagnetizing effect upon the square loop materials. Properly designed transformers using "cut" toroid or "C-core" square loop materials will not saturate upon turn-on and can tolerate a certain amount of unbalanced drive or dc excitation.

It should be emphasized, however, that because of the nature of the material and the small size of the gap, extreme care and control must be taken in performing the gapping operation, otherwise the desired shearing effect will not be achieved and the low-loss properties destroyed. The cores must be very carefully cut, lapped, and etched to provide smooth, residue-free surfaces. Reassembly must be performed with equal care.

BIBLIOGRAPHY

Brown, A. A., et al., Cyclic and Constant Temperature Aging Effects on Magnetic Materials for Inverters and Converters, NASA CR-(L-80001). National Aeronautics and Space Administration, Washington, June 1969.

Design Manual Featuring Tape Wound Cores, TWC-300. Magnetic Inc., Butler, Pa., 1962.

Frost, R. M., et al., Evaluation of Magnetic Materials for Static Inverters and Converters, NASA CR-1226. National Aeronautics and Space Administration, Washington, February 1969.

Lee, R., Electronic Transformers and Circuits, Second Edition. John Wiley & Sons, New York, 1958.

Nordenberg, H. M., Electronic Transformers. Reinhold Publishing Co., New York, 1964.

Platt, S., Magnetic Amplifiers: Theory and Application. Prentice-Hall, Englewood Cliffs, N. J., 1958.

Flight Projects, Space Programs Summary 37-64, Vol. I, p. 17. Jet Propulsion Laboratory, Pasadena, Calif., July 31, 1970.

Technical Data on Arnold Tape-Wound Cores, TC-101A. Arnold Engineering, Marengo, Ill., 1960.

Table 1. Magnetic core material characteristics

Trade names	Composition	Saturated flux density, T[1]	DC coercive force, A-t/cm	Squareness ratio	Material density, g/cm^3	Loss factor at 3 kHz and 0.5 T, W/kg
Magnesil Silectron Microsil Supersil	3% Si 97% Fe	1.5-1.8	0.5-0.75	0.85-1.0	7.63	33.1
Deltamax Orthonol 49 Sq. Mu	50% Ni 50% Fe	1.4-1.6	0.125-0.25	0.94-1.0	8.24	17.66
Allegheny 4750 48 Alloy Carpenter 49	48% Ni 52% Fe	1.15-1.4	0.062-0.187	0.80-0.92	8.19	11.03
4-79 Permalloy Sq. Permalloy 80 Sq. Mu 79	79% Ni 17% Fe 4% Mo	0.66-0.82	0.025-0.05	0.80-1.0	8.73	5.51
Supermalloy	78% Ni 17% Fe 5% Mo	0.65-0.82	0.0037-0.01	0.40-0.70	8.76	3.75

[1] 1 T = 10^4 G

[2] 1 g/cm^3 = 0.036 lb/in.^{3}

Table 2. Materials and constraints

Core type	Material	B_m, T	N_T	Frequency, Hz	$m\ell$, cm
52029 (2A)	Orthonol	1.	54	2.4	9.47
52029 (2D)	Sq. Permalloy	0.75	54	2.4	9.47
52029 (2F)	Supermalloy	0.75	54	2.4	9.47
52029 (2H)	48-Alloy	1.15	54	2.4	9.47
52029 (2H)	Magnesil	1.6	54	2.4	9.47

Table 3. Comparing B_r/B_m on uncut and cut cores

Code	Material	Uncut B_r/B_m	Cut B_r/B_m
(A)	Orthonol	0.96	0.62
(D)	Mo-Permalloy	0.86	0.21
(K)	Magnesil	0.93	0.22
(F)	Supermalloy	0.81	0.24
(H)	48 Alloy	0.83	0.30

Table 4. Comparing $\Delta H - \Delta H_{OP}$ on uncut and cut cores

Material	B_m, T	B_{ac}, T	B_{dc}, T	Uncut		Cut	
				ΔH_{OP}	ΔH	ΔH_{OP}	ΔH
				A-t/cm			
Orthonal	1.44	1.15	0.288	0.0125	0.0	0.895	0.178
48 Alloy	1.12	0.89	0.224	0.0250	0.0	1.60	0.350
Sq. Permalloy	0.73	0.58	0.146	0.01	0.005	0.983	0.178
Supermalloy	0.68	0.58	0.136	0.0175	0.005	0.491	0.224
Magnesil	1.54	1.23	0.31	0.075	0.025	7.15	1.78

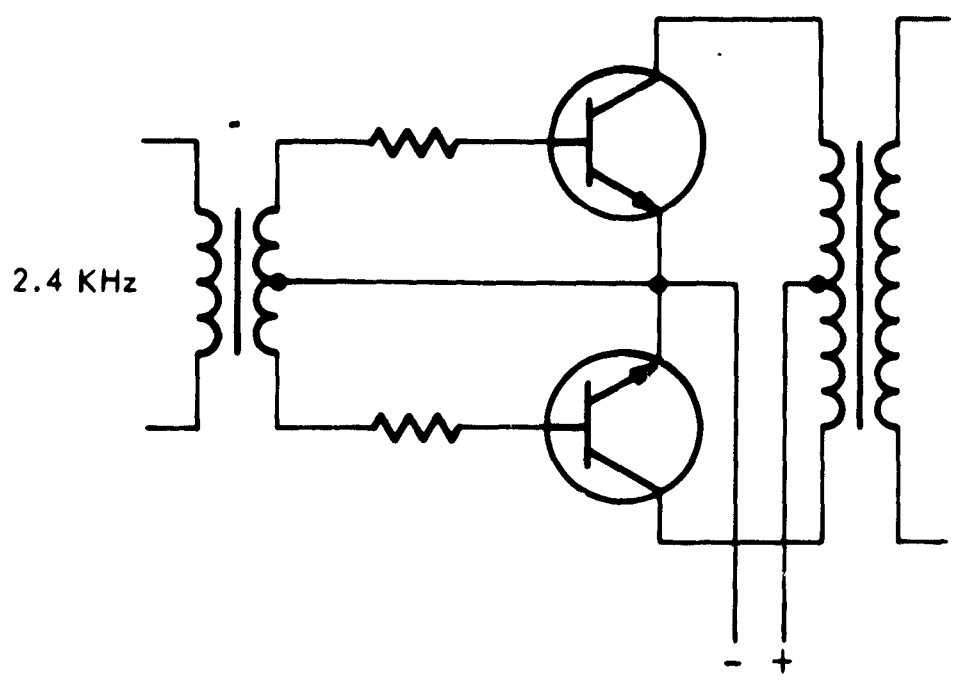

Fig. 1. Typical driven transistor inverter

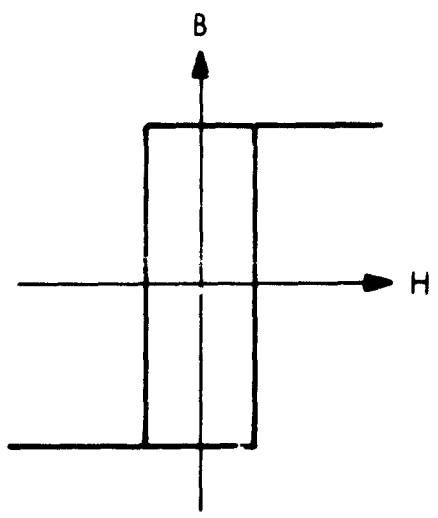

Fig. 2. Ideal square B-H loop

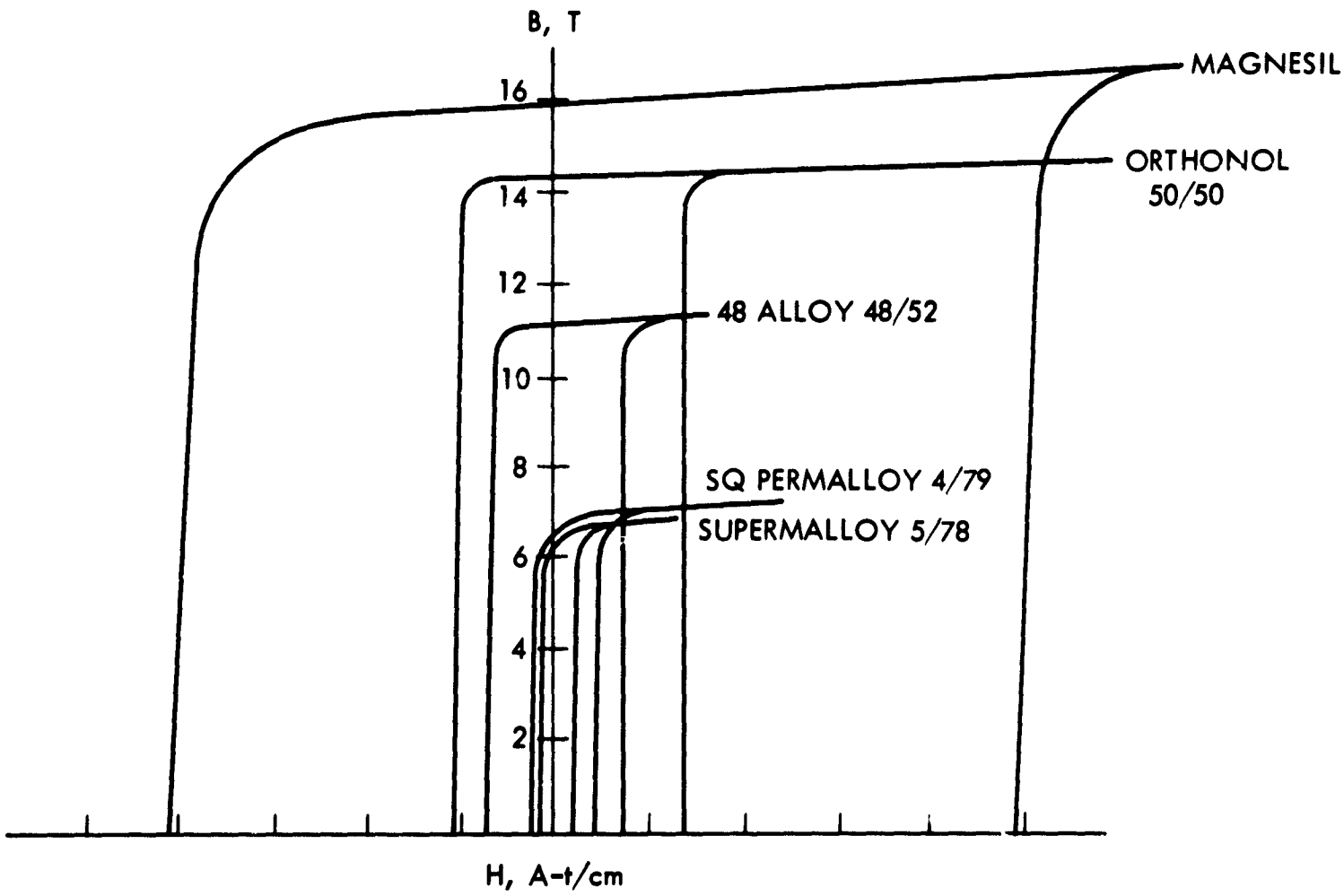

Fig. 3. The typical dc B-H loops of magnetic materials

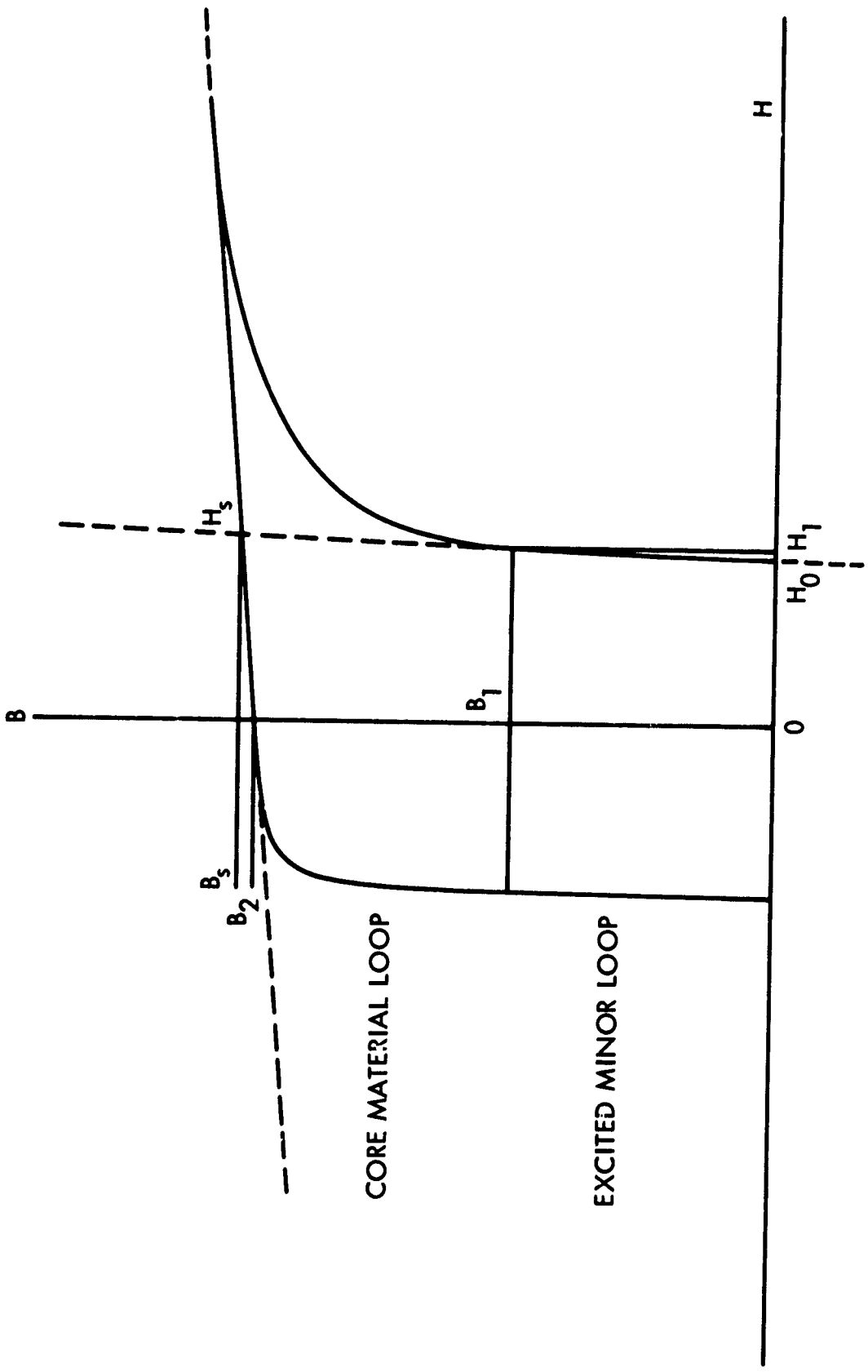

Fig. 4. Defining the B-H loop

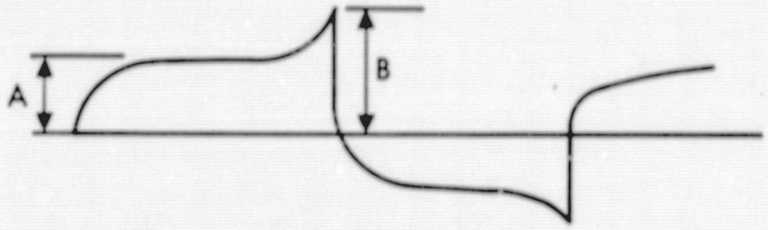

SATURATION OCCURS WHEN B = 2A

Fig. 5. Excitation current

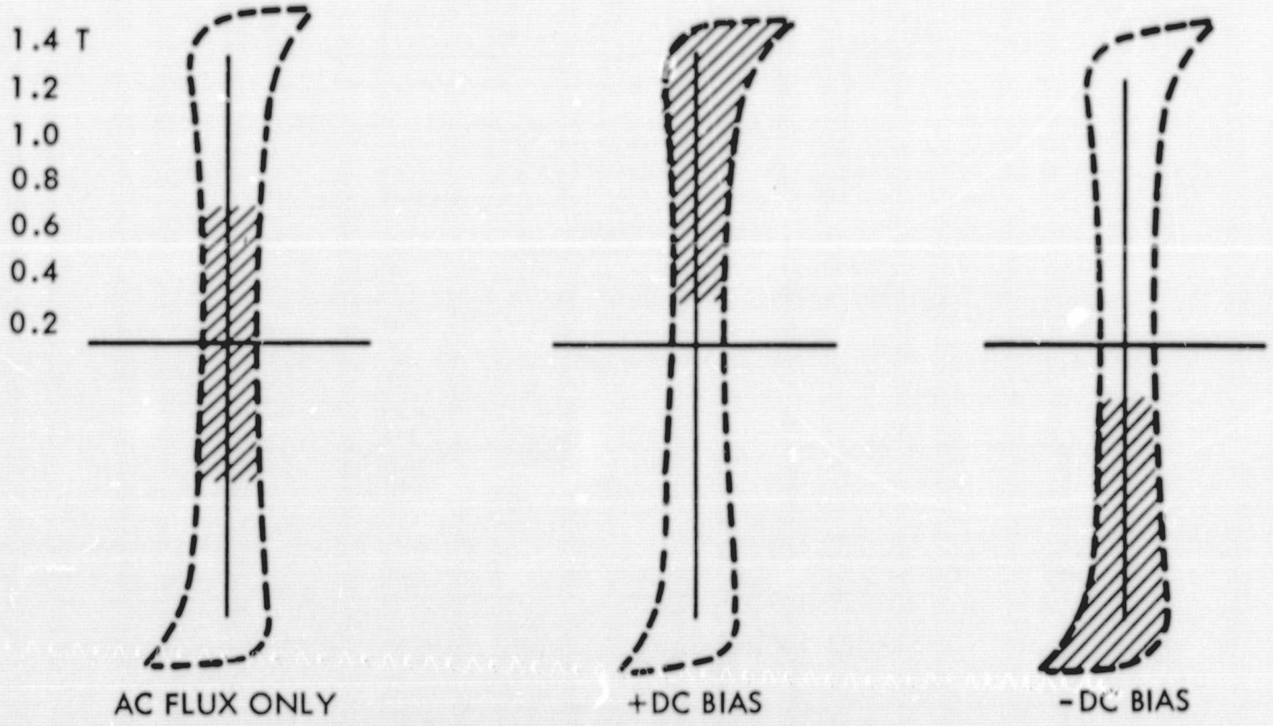

Fig. 6. B-H loop with dc bias

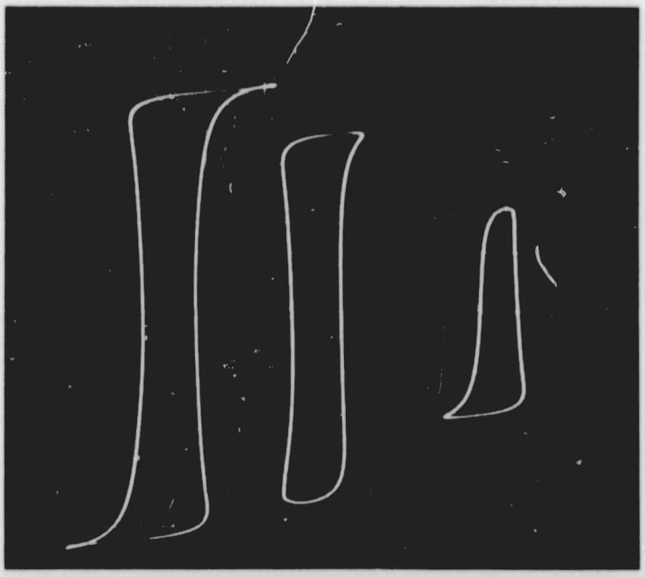

Fig. 7. Typical square loop material with ac excitation

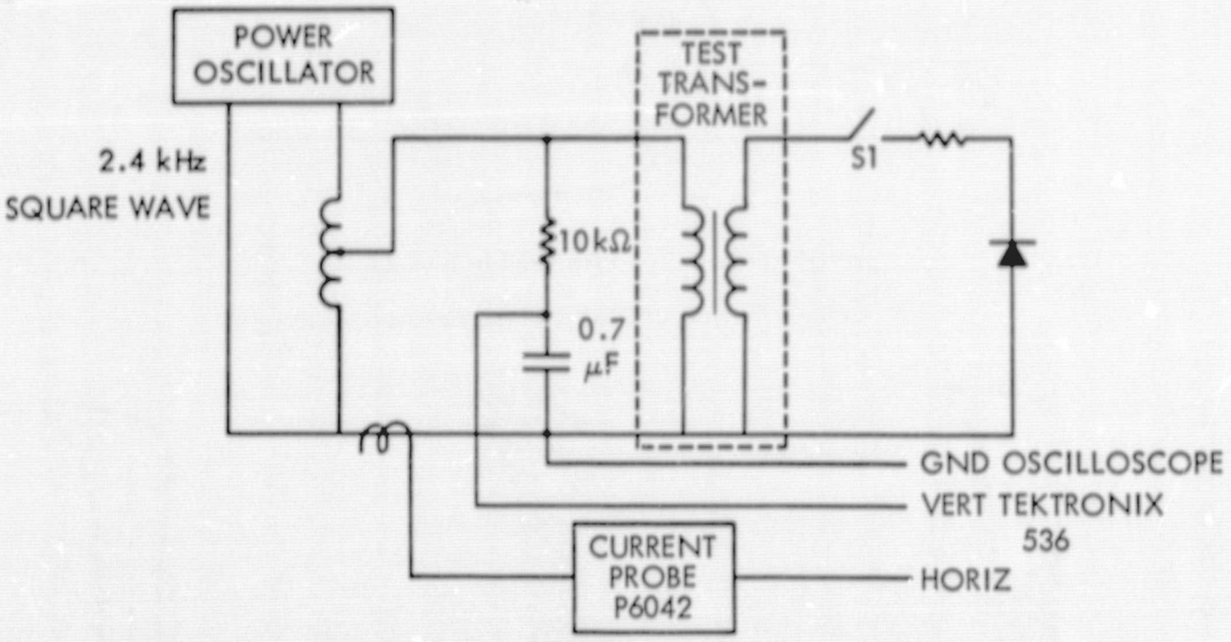

Fig. 8. Dynamic B-H loop test fixture

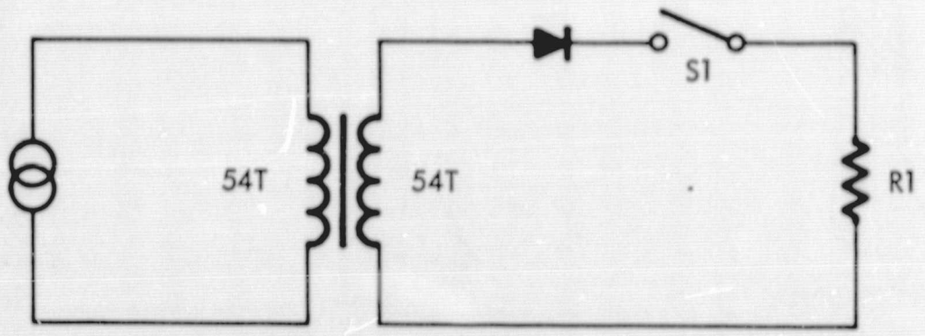

Fig. 9. Implementing dc unbalance

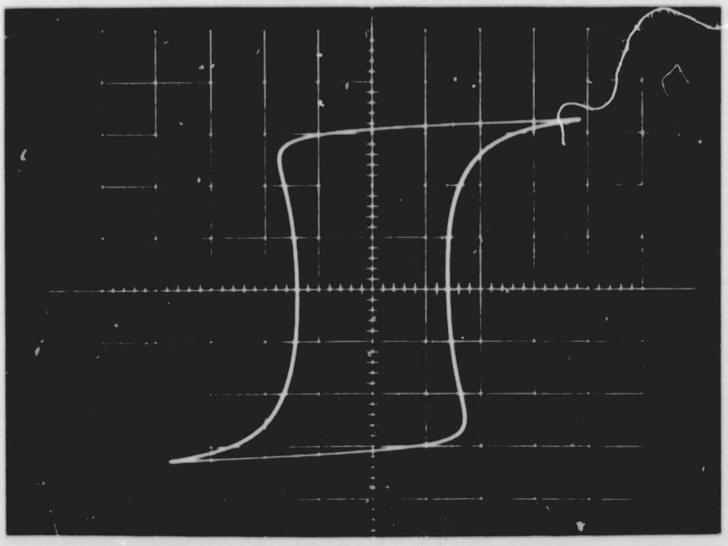

VERT = 0.5 T/cm
HORIZ = 100 mA/cm

Fig. 10. Magnesil (K) B-H loop

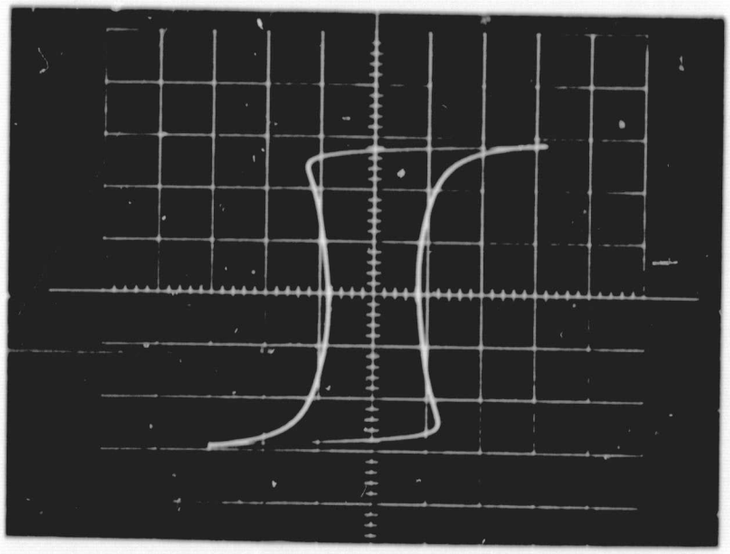

VERT = 0.5 T/cm
HORIZ = 50 mA/cm

Fig. 11. Orthonol (A) B-H loop

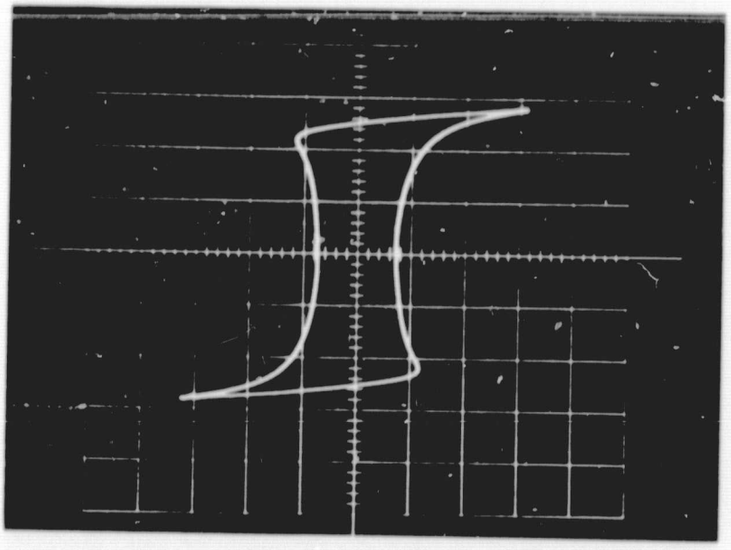

VERT = 0.5 T/cm
HORIZ = 50 mA/cm

Fig. 12. 48 Alloy (H) B-H loop

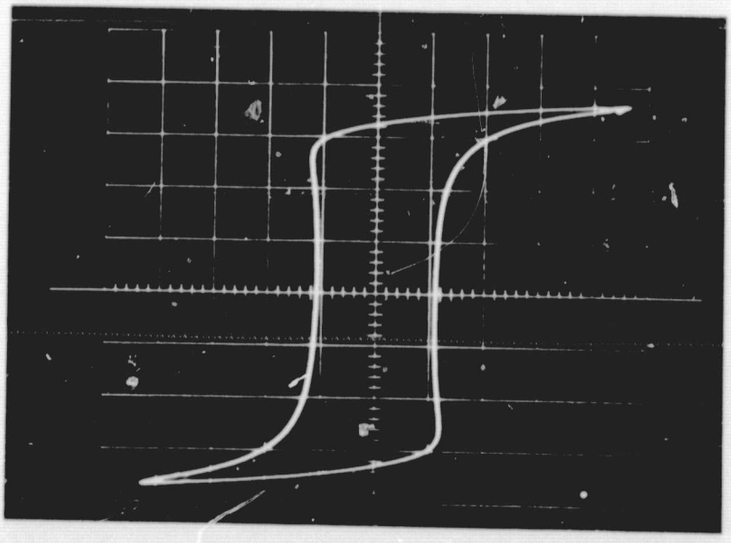

VERT = 0.2 T/cm
HORIZ = 10 mA/cm

Fig. 13. Sq. Permalloy (P) B-H loop

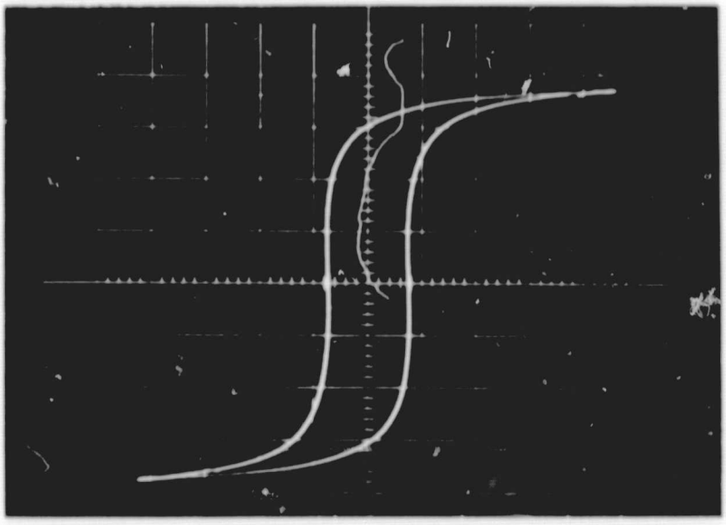

Fig. 14. Supermalloy (F) B-H loop

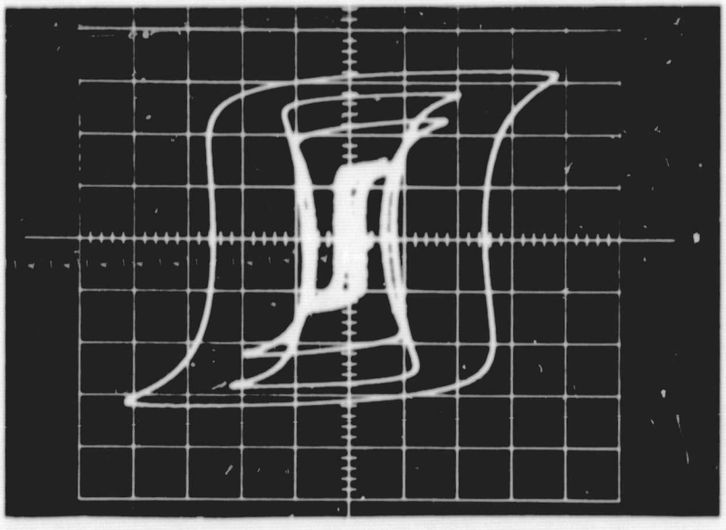

Fig. 15. Composite 52029 (2K), (A), (H), (P), and (F) B-H loops

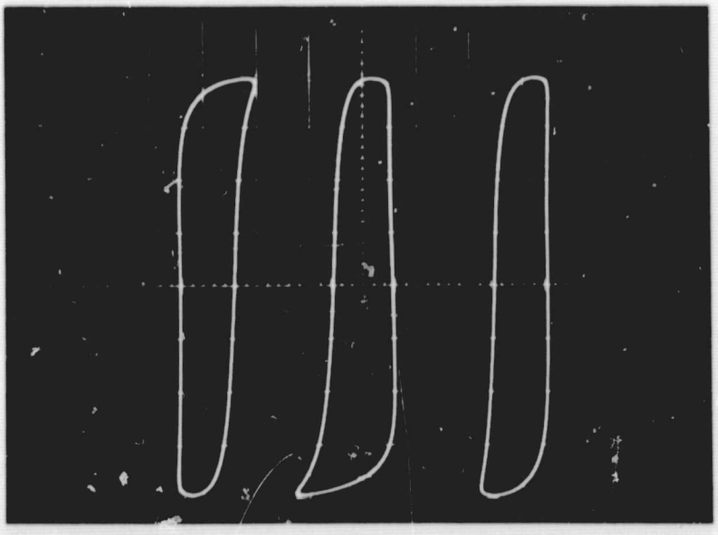

Fig. 16. Magnesil (K) B-H loop with and without dc

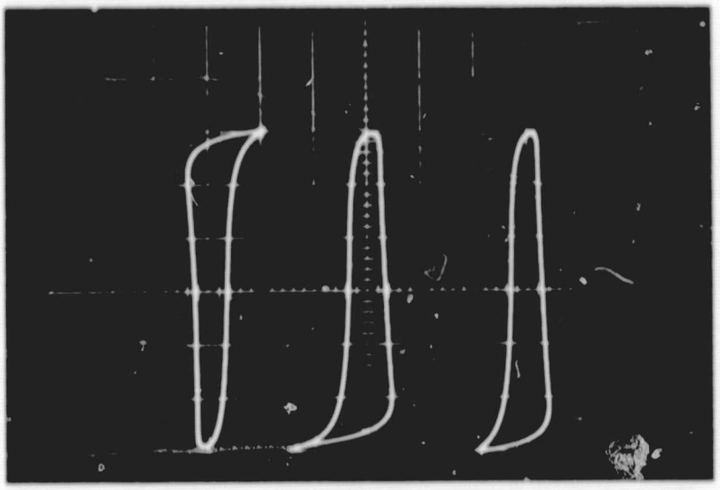

VERT = 100 mA/cm
HORIZ = 0.2 T/cm

Fig. 17. Orthonol (A) B-H loop with and without dc

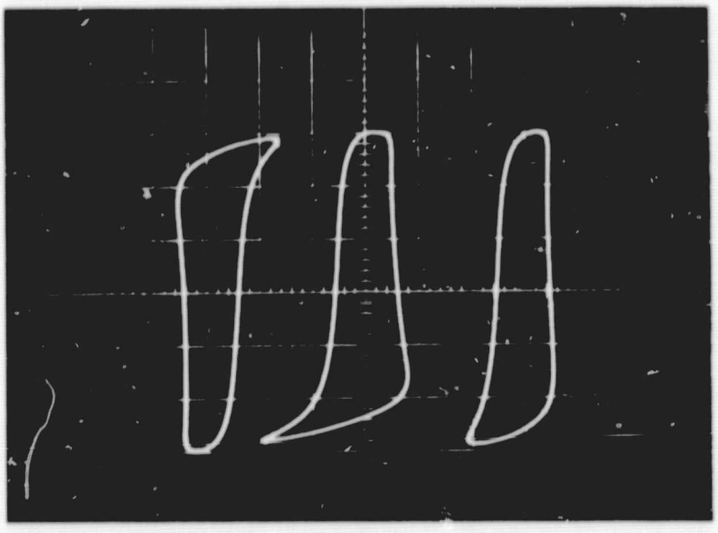

VERT = 50 mA/cm
HORIZ = 0.2 T/cm

Fig. 18. 48 Alloy (H) B-H loop with and without dc

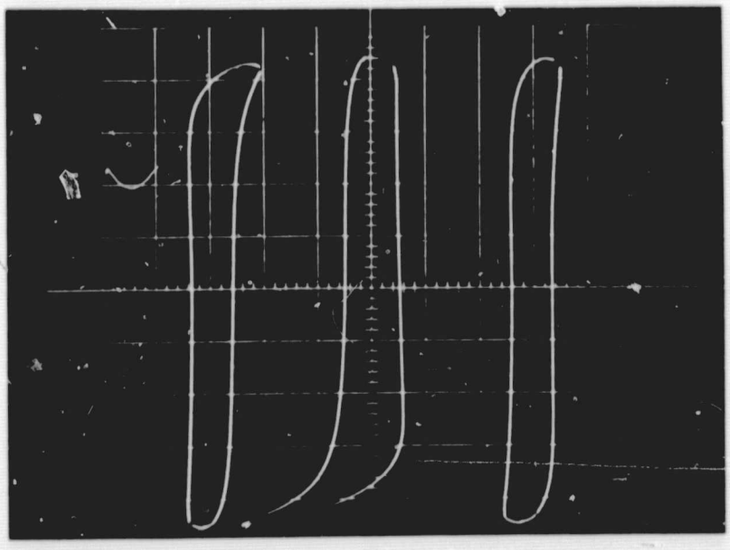

VERT = 20 mA/cm
HORIZ = 0.1 T/cm

Fig. 19. Sq. Permalloy (P) B-H loop with and without dc

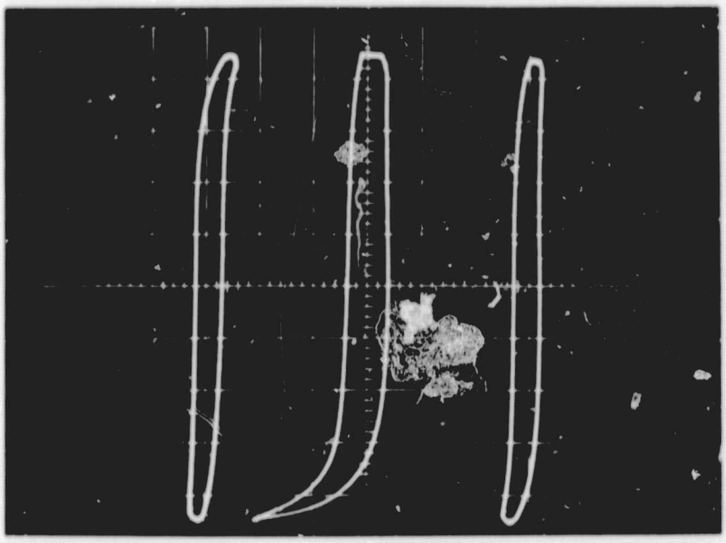

Fig. 20. Supermalloy (F) B-H loop with and without dc

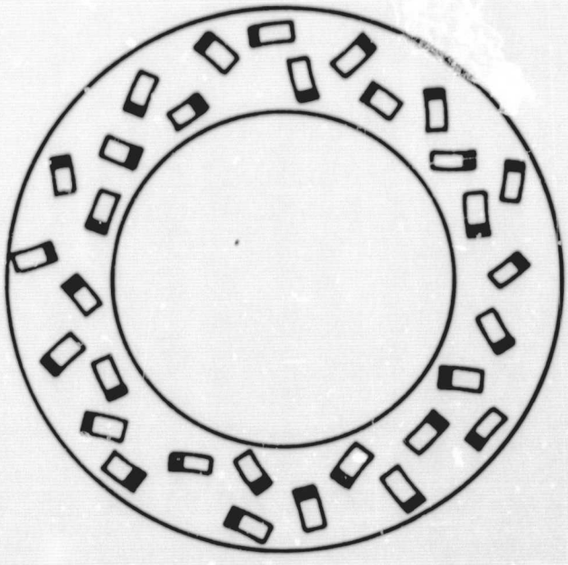

Fig. 21. Unmagnetized material

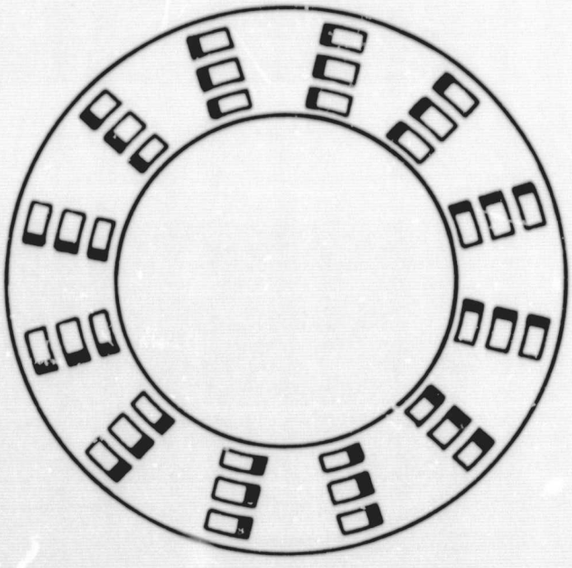

Fig. 22. Magnetized material

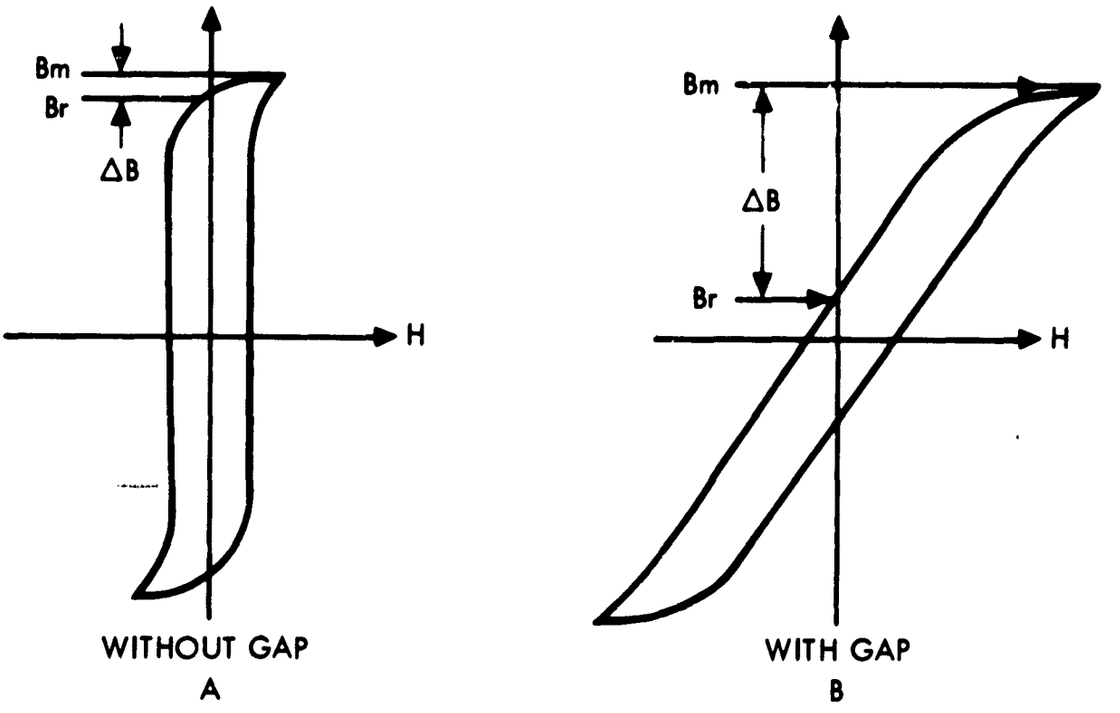

Fig. 23. Air gap increases the effective length of the magnetic path

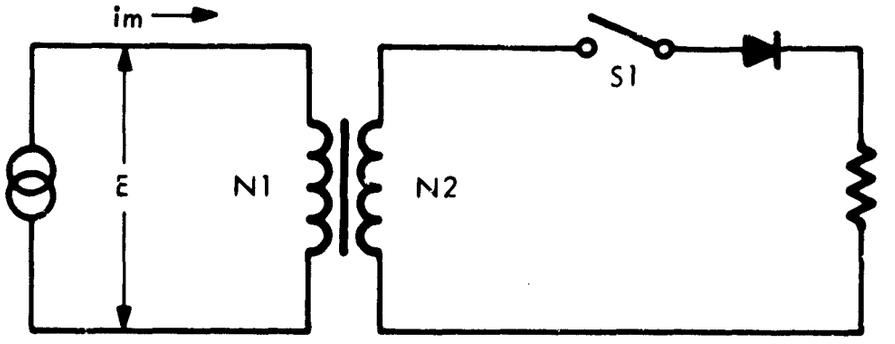

Fig. 24. Implementing dc unbalance

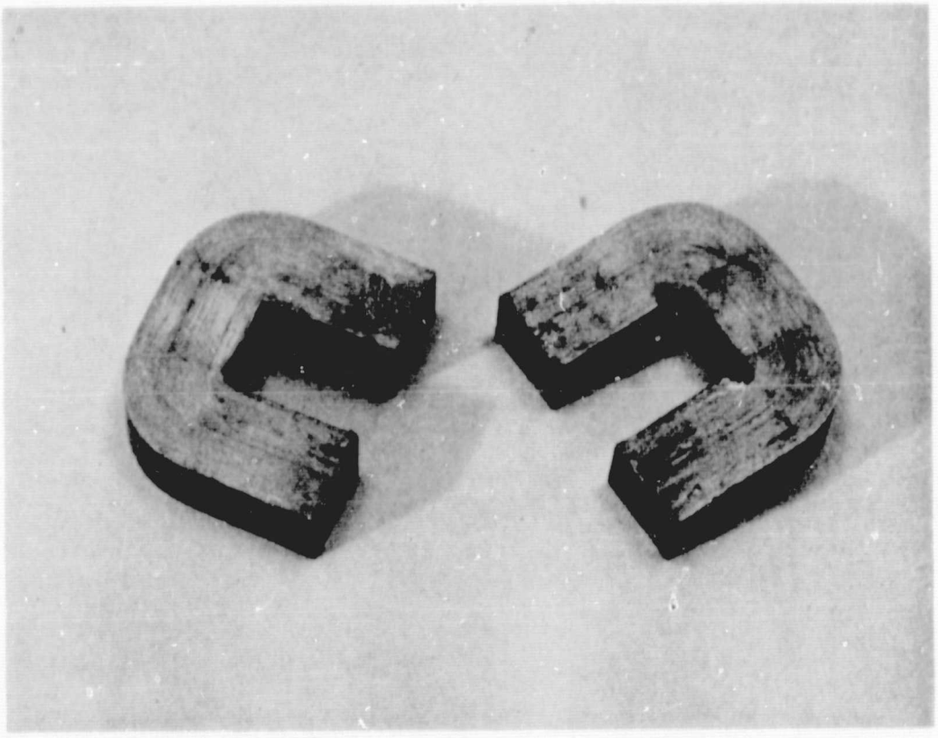

Fig. 25. Typical cut toroid

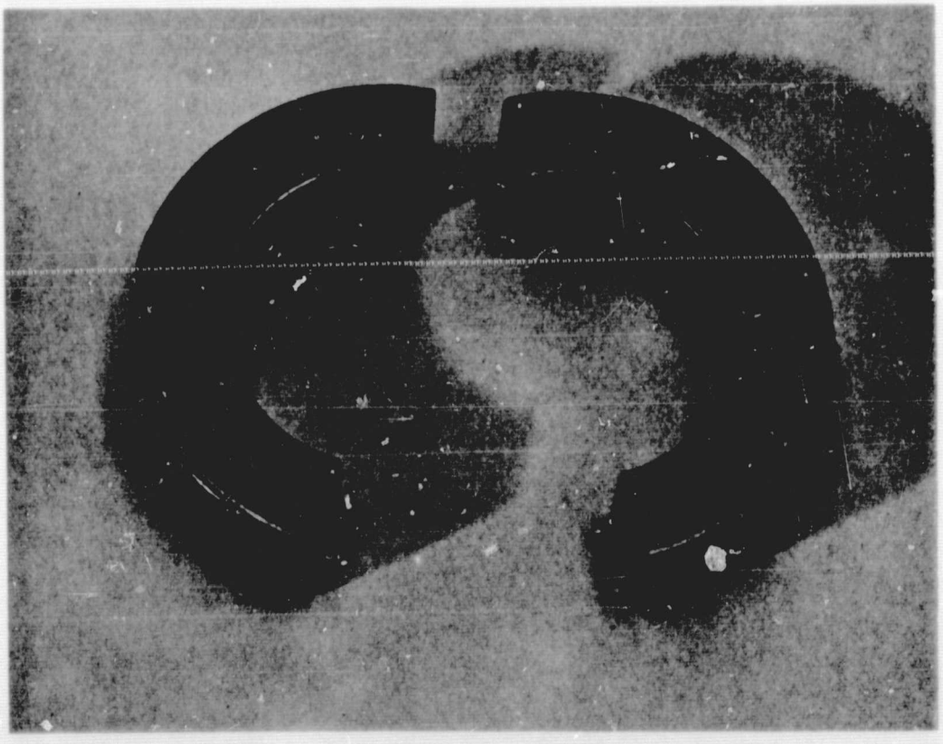

Fig. 26. Typical cut "C" core

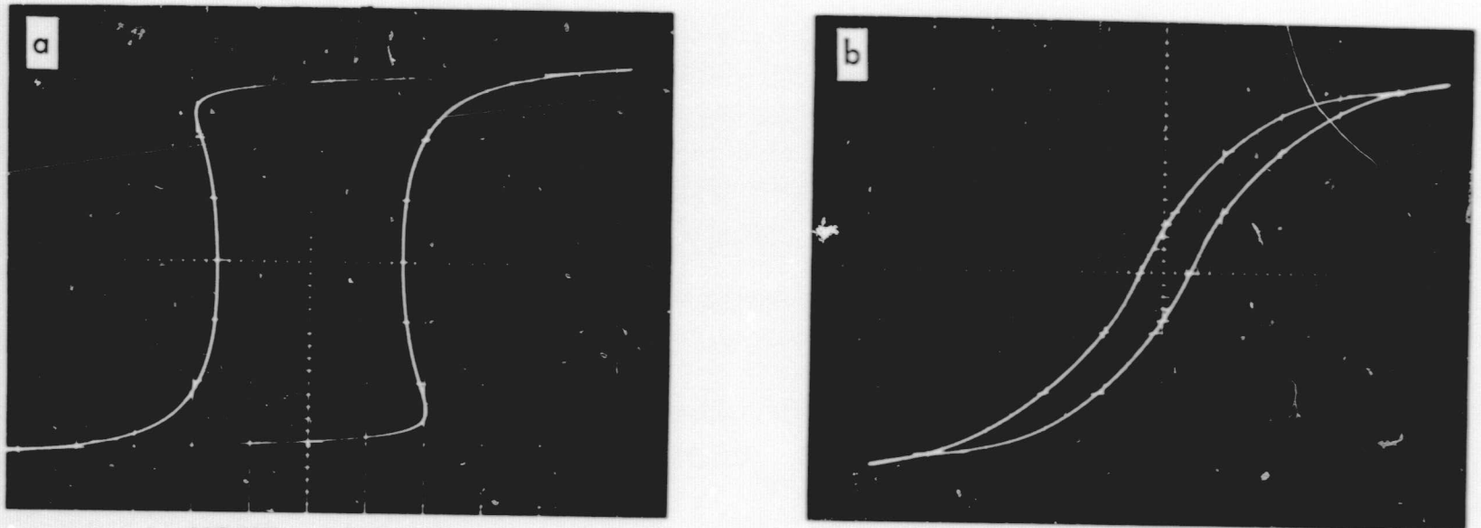

Fig. 27. Magnesil 52029 (2K) B-H loop, (a) uncut and (b) cut

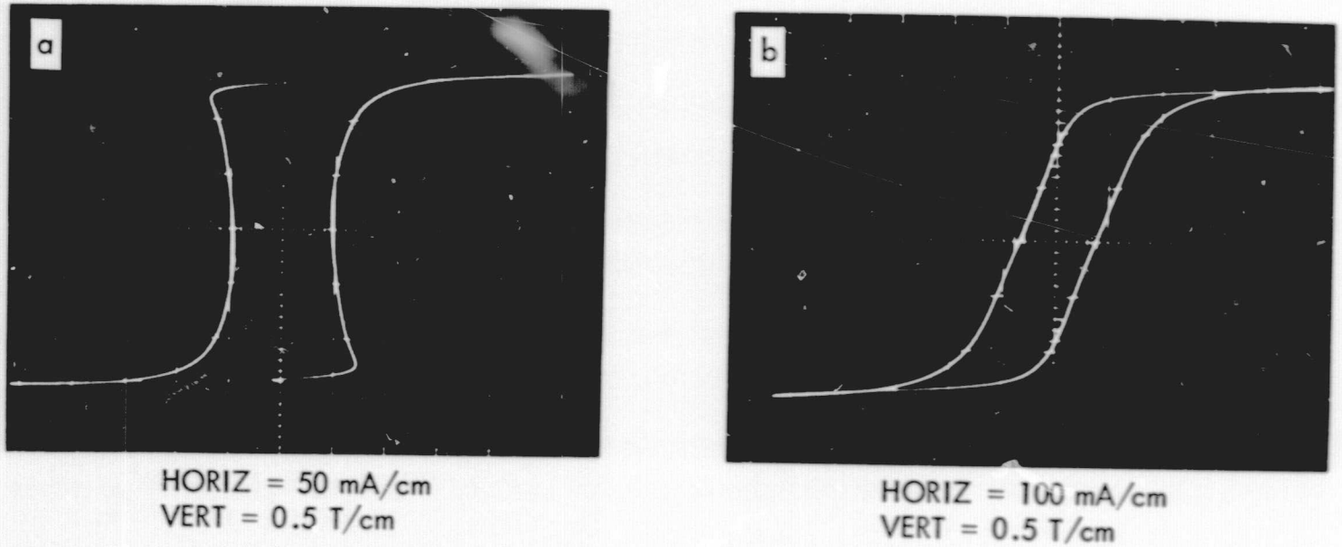

Fig. 28. Orthonol 52029 (2A) B-H loop, (a) uncut and (b) cut

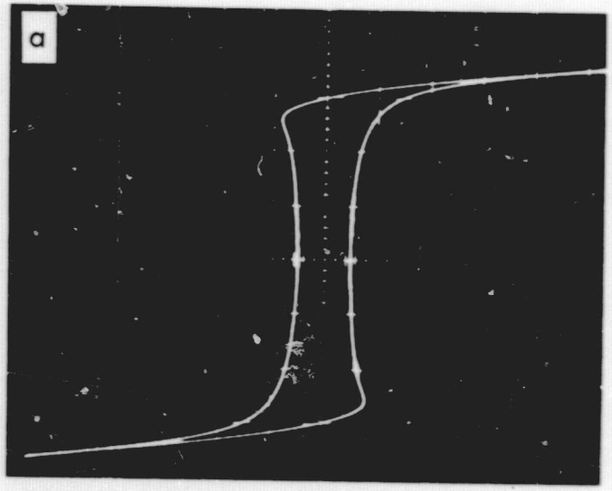

HORIZ = 100 mA/cm
VERT = 0.3 T/cm

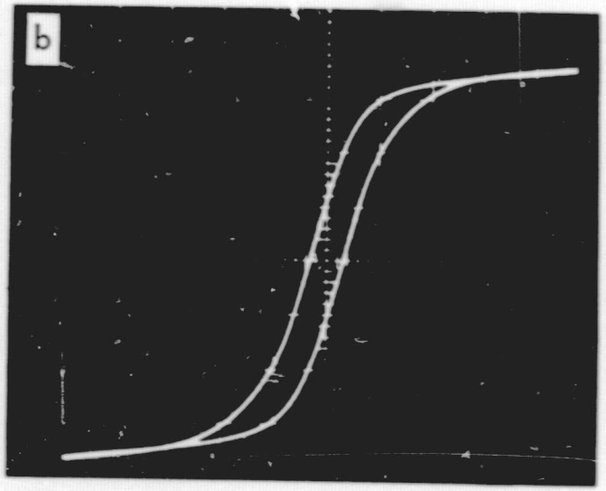

HORIZ = 200 mA/cm
VERT = 0.3 T/cm

Fig. 29. 48 Alloy 52029 (2H) B-H loop, (a) uncut and (b) cut

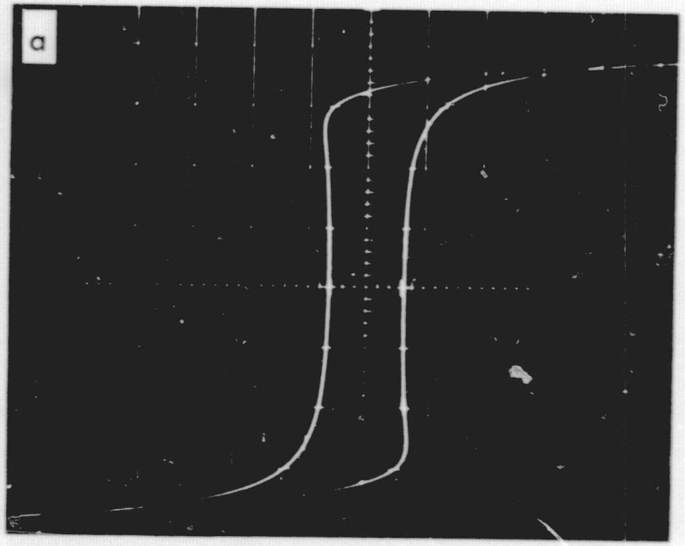

HORIZ = 20 mA/cm
VERT = 0.2 T/cm

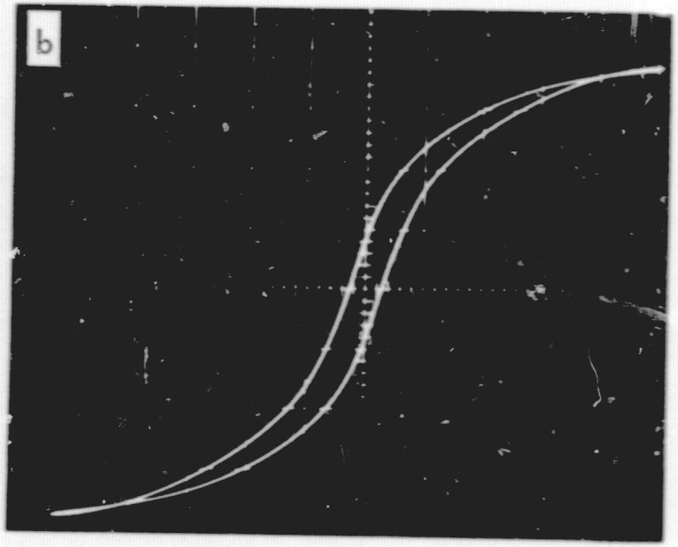

HORIZ = 100 mA/cm
VERT = 0.2 T/cm

Fig. 30. Sq. Permalloy 52029 (2D) B-H loop, (a) uncut and (b) cut

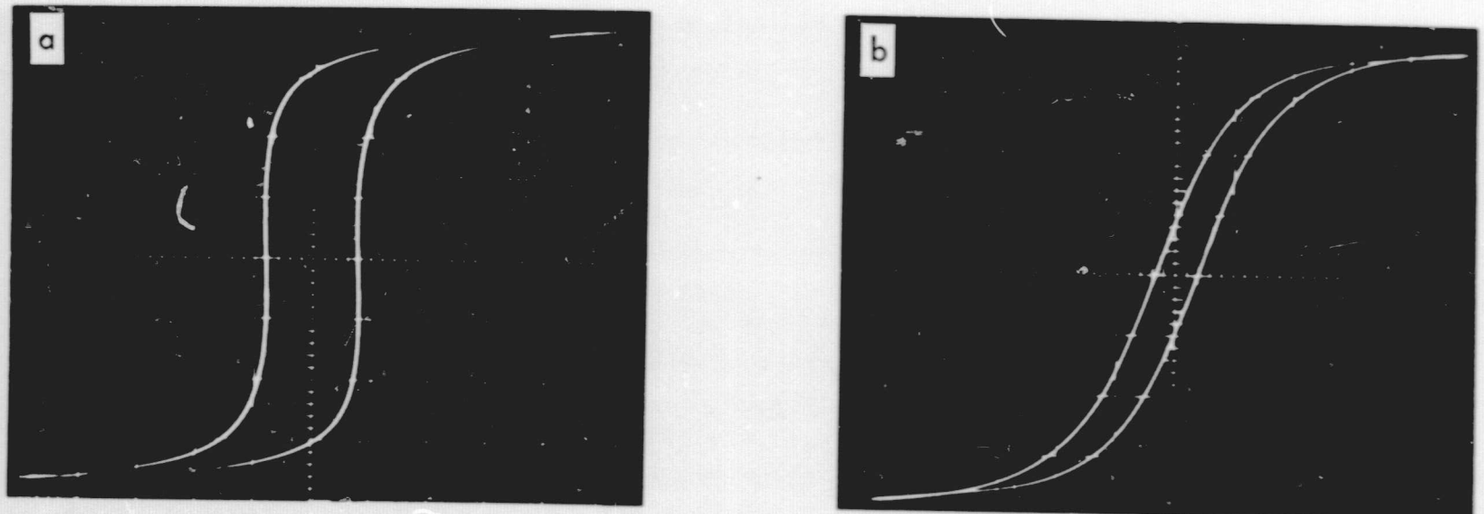

Fig. 31. Supermalloy 52029 (2F) B-H loop, (a) uncut and (b) cut

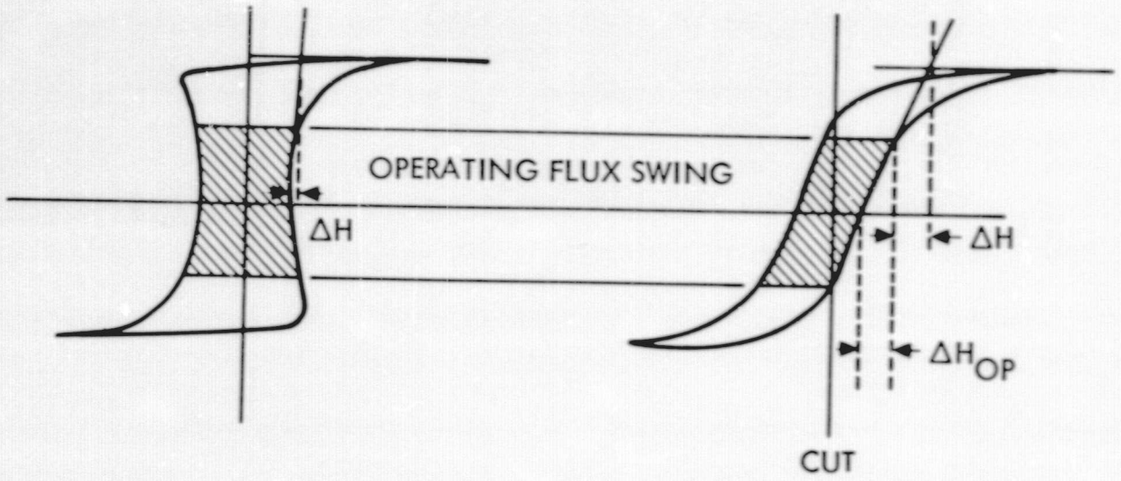

Fig. 32. Defining ΔH and ΔH_{OP}

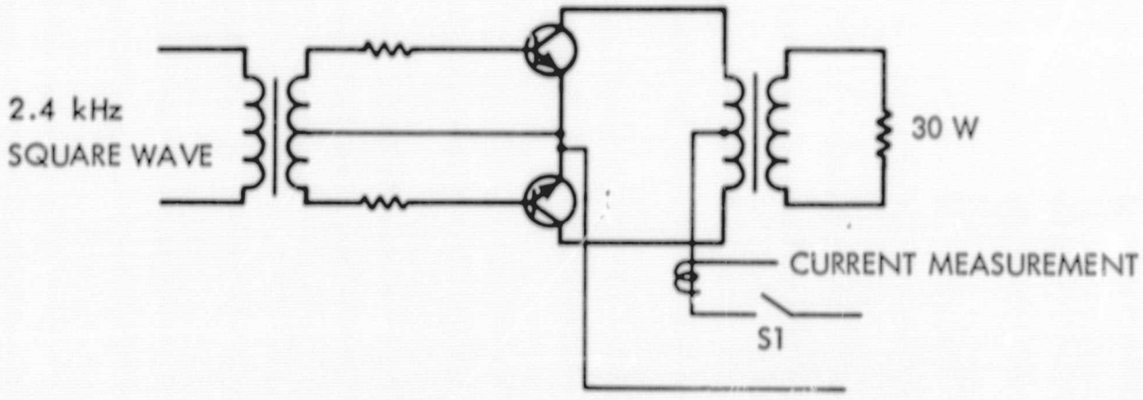

Fig. 33. Inverter inrush current measurement

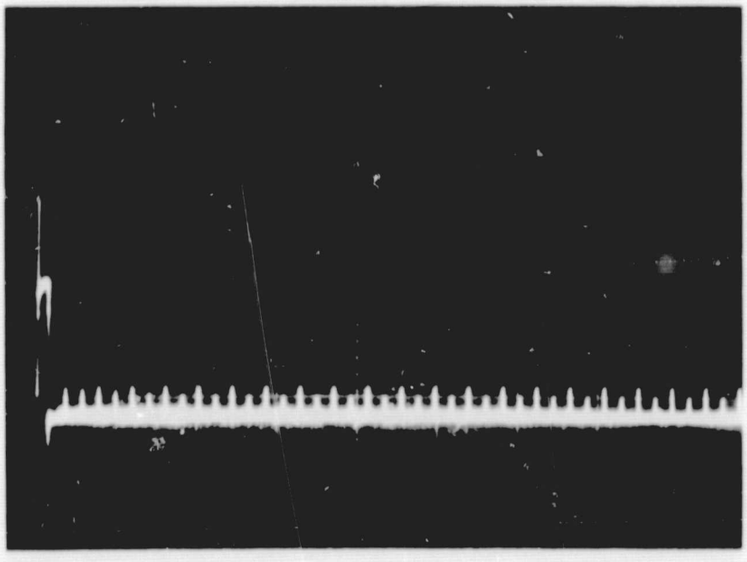

Fig. 34. Typical inrush of an uncut core in a driven inverter

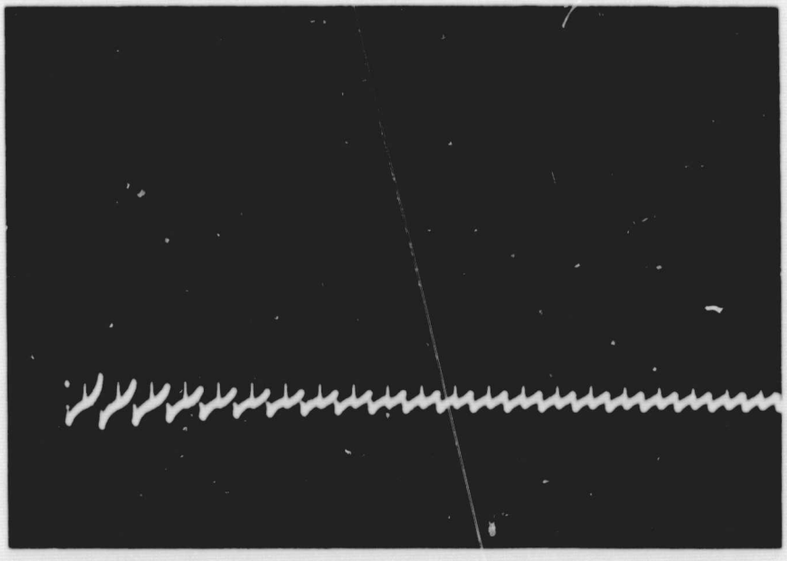

Fig. 35. Typical inrush current of a cut core in a driven inverter

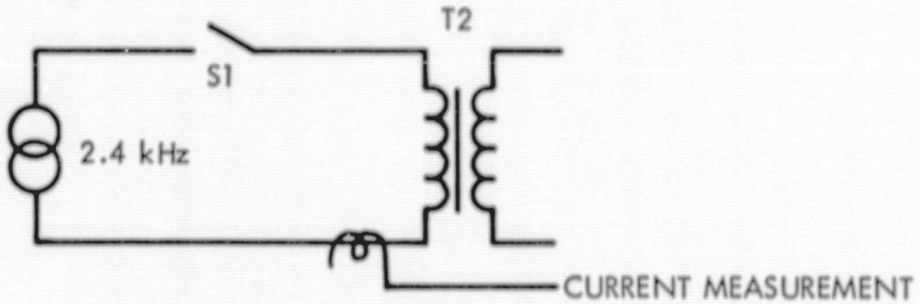

Fig. 36. T-R supply current measurement

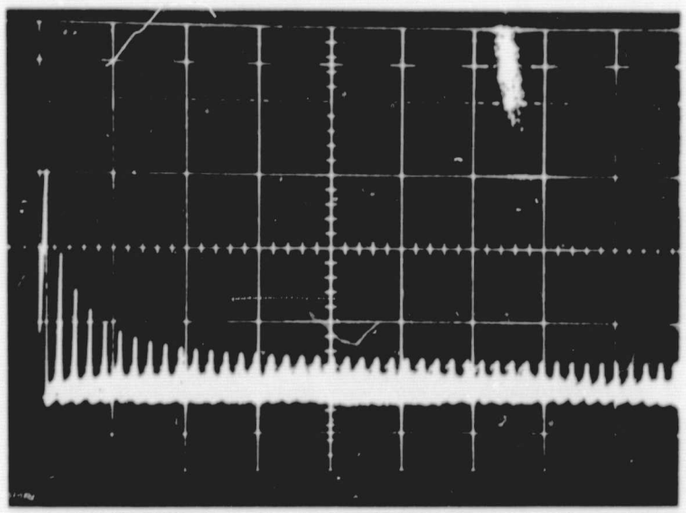

Fig. 37. Typical inrush current of an uncut core operating from an ac source

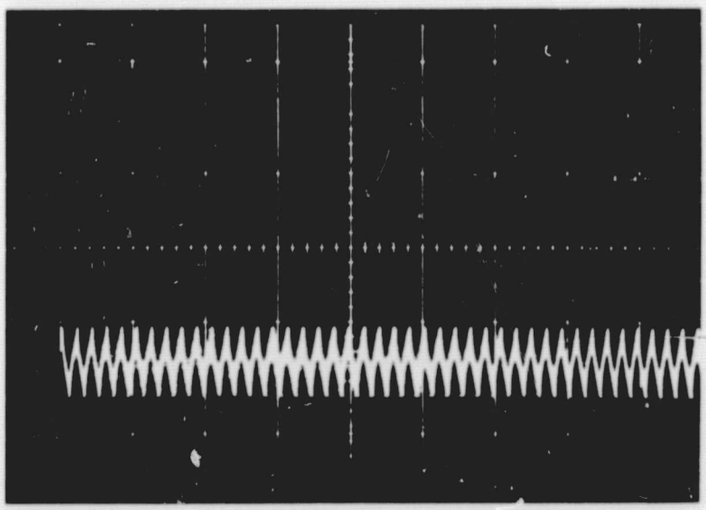

Fig. 38. Typical inrush current of a cut core in a T-R

NASA — JPL — Coml., L.A., Calif.